Inelastic Proton-Proton Scattering at 1.35, 2.1, and 2.9 BeV*†

G. B. CHADWICK,‡ G. B. COLLINS, P. J. DUKE,§ T. FUJII, N. C. HIEN,‖ M. A. R. KEMP,§ AND F. TURKOT
Brookhaven National Laboratory, Upton, New York

(Received July 10, 1962; revised manuscript received August 21, 1962)

Absolute measurements have been made of the momentum spectrum of protons inelastically scattered from protons at incident kinetic energies of 1.35, 2.1, and 2.9 BeV, and at angles from 2° to 17° in the laboratory system. Peaks in these spectra were found at momenta corresponding to excitation of the resonances occurring in π-p scattering at 180-, 600-, and 900-MeV laboratory kinetic energies. A simple calculation of the inelastic spectra based on the one-pion-exchange (OPE) model is presented, and found to be in general agreement with the experimental data for values of the square of the invariant four-momentum transfer, Δ^2, less than $6m_\pi^2$. For larger values of Δ^2 the theory overestimates. When values of the differential cross section at the position of the $J=T=3/2$ resonance are compared with predictions of the OPE calculation, the ratio is found to be a smooth function of Δ^2 out to a value of $55m_\pi^2$, the limit reached in this experiment. To within 20% this ratio appears to be independent of incident proton energy for our range of observation. The differential cross sections at the peaks corresponding to the $T=1/2$ resonances are closer to the theoretical values than for the $T=3/2$ resonance, for the same value of Δ^2.

I. INTRODUCTION

ALTHOUGH p-p interactions in the few BeV region have been available for experimental study for nearly a decade now, it is only in the past few years that a quantitative understanding of certain aspects of this interaction has been achieved. The early cloud chamber experiments[1] on pion production, despite limited statistics, clearly established the inadequacies of the Fermi statistical theory in this energy range. They also suggested the path of subsequent developments by exhibiting two prominent characteristics of inelastic interactions: (a) the importance of the 3, 3 ($T=J=3/2$) pion-nucleon resonance, and (b) the tendency for forward-backward peaking of the nucleons in the c.m. system. The first characteristic was incorporated in an isobar model for inelastic nucleon-nucleon collisions proposed by Lindenbaum and Sternheimer.[2] This model has achieved a notable success in fitting the c.m. energy distributions, averaged over angle, of the final-state particles in single and double meson production.[3–7] Since this isobar model does not postulate a specific mechanism for excitation of the isobar it is incapable of predicting absolute cross sections, the dependence on incident energy, and the angular distributions. The basis for a more quantitative theory originated with the work of Goebel[8] and Chew and Low,[9] who pointed out the importance of one-particle-exchange pole terms in the production amplitudes for small values of momentum transfer, Δ. The fact that experiments clearly indicated a preference for small momentum transfer led many people[10] to formulate a model of high-energy collisions on this basis; because of the pole approximation, this theory is expected to describe only peripheral collisions.

The experiment to be described here is a continuation of a previous work of the authors[11] in observing the inelastic proton spectrum resulting from p-p collisions by counter techniques. This earlier work provided a clear demonstration of peaks in the inelastic spectra corresponding to formation of the 3, 3 isobar.

A number of recent bubble chamber experiments[4,6,12] on p-p collisions in the 1–3-BeV region have provided more detailed information on the inelastic interactions, but with statistical limitations concomitant to that technique. The single pion production data have been interpreted in terms of the one-pion-exchange (OPE) model as developed by Selleri[12–14]; the absolute agreement for $\Delta^2<4\mu^2$ ($\mu=m_\pi$) is impressive, but the theory systematically overestimates for larger Δ^2. Although the limitations of the simple OPE pole formulas are now apparent, the precise role of the one-pion-exchange

* Work performed under the auspices of the U. S. Atomic Energy Commission.

† A thesis based on a part of this work has been submitted to the Carnegie Institute of Technology by N. C. Hien in partial fulfillment of the requirements for the degree of Doctor of Philosophy.

‡ Present address: the Clarendon Laboratory, Oxford University, Oxford, England.

§ On leave from National Institute for Research in Nuclear Science, Harwell, England.

‖ Present address: Carnegie Institute of Technology, Pittsburgh, Pennsylvania.

[1] W. B. Fowler, R. P. Shutt, A. M. Thorndike, W. L. Whittemore, V. T. Cocconi, E. Hart, M. M. Block, E. M. Harth, E. C. Fowler, J. D. Garrison, and T. W. Morris, Phys. Rev. **103**, 1489 (1956).

[2] S. J. Lindenbaum and R. M. Sternheimer, Phys. Rev. **105**, 1874 (1957).

[3] For references to single production see R. M. Sternheimer, and S. J. Lindenbaum, Phys. Rev. **123**, 333 (1961).

[4] W. J. Fickinger, E. Pickup, D. K. Robinson, and E. O. Salant, Phys. Rev. **125**, 2082 (1962).

[5] E. Pickup, D. K. Robinson, and E. O. Salant, Phys. Rev. **125**, 2091 (1962).

[6] G. A. Smith, H. Courant, E. C. Fowler, H. Kraybill, J. Sandweiss, and H. Taft, Phys. Rev. **123**, 2160 (1961).

[7] E. L. Hart, R. I. Louttit, D. Luers, T. W. Morris, W. J. Willis, and S. S. Yamamoto, Phys. Rev. **126**, 747 (1962).

[8] C. Goebel, Phys. Rev. Letters **1**, 337 (1958).

[9] G. F. Chew and F. E. Low, Phys. Rev. **113**, 1640 (1959).

[10] For a concise review of this model and references to the literature see S. D. Drell, Revs. Modern Phys. **33**, 458 (1961).

[11] G. B. Chadwick, G. B. Collins, C. E. Swartz, A. Roberts, S. deBenedetti, N. C. Hien, and P. J. Duke, Phys. Rev. Letters **4**, 611 (1960).

[12] V. E. Barnes, D. V. Bugg, W. P. Dodd, J. B. Kinson, and L. Riddiford, Phys. Rev. Letters **7**, 288 (1961).

[13] F. Selleri, Phys. Rev. Letters **6**, 64 (1961).

[14] W. J. Fickinger, E. Pickup, D. K. Robinson, and E. O. Salant, Phys. Rev. Letters **7**, 196 (1961).

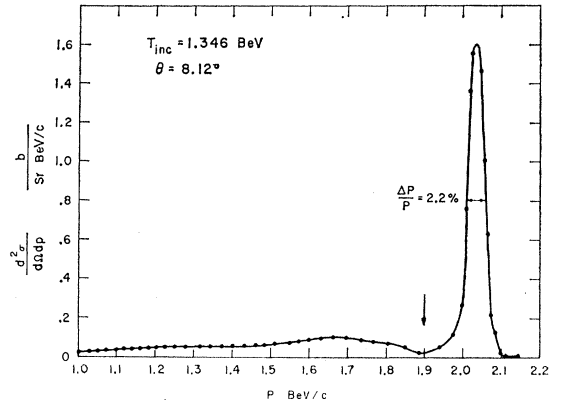

FIG. 1. Typical laboratory momentum spectrum of secondary protons from p-p scattering. The arrow denotes the kinematic limit for inelastic protons.

process, as well as that of other possible exchanges, remains an open question. The motivation for the present experiment was to obtain absolute differential cross sections of high statistical accuracy over a wide range of Δ^2; a further objective was to seek direct evidence of the higher nucleon isobars.

In this experiment, the external beam of the Cosmotron was passed through a liquid-hydrogen target; the scattered protons emerging at a fixed laboratory angle were momentum analyzed by means of a magnetic spectrometer and scintillation counters. A typical momentum spectrum obtained in this way is shown in Fig. 1; this example is for an incident energy of 1.35 BeV and a scattering angle of 8.1°. The lowest momentum measured corresponds to protons nearly at rest in the c.m. system of the initial protons. The peak at the right arises from elastic scattering; the cross sections and analysis of the elastic data are contained in an accompanying article.[15] With the exception of the 1.35-BeV data, the inelastic spectrum is a composite of contributions from a number of inelastic channels. The feature which greatly simplifies a quantitative comparison with the predictions of the OPE model in this complex situation is that there is a region, approximately 200 MeV/c wide, at the upper end of each inelastic spectrum to which only single-pion production can contribute. Although the OPE model can also treat multi-pion production, any comparison with an experiment of this nature will clearly be more difficult.

Single production in p-p collisions occurs through the following two channels:

$$p+p \rightarrow p+p+\pi^0, \tag{1.1}$$

$$p+p \rightarrow p+n+\pi^+. \tag{1.2}$$

The Feynman diagram for reaction (1.1) in the OPE model is given in Fig. 2. In this model the virtual π^0, which transfers four momentum Δ between the two vertices, is assumed to behave like a real pion at the right vertex, thus enabling the substitution of the experimental π^0-p elastic differential cross section in calculating this diagram. The total energy, W, in the c.m. system of the π^0-p scattering event is determined by $\mathbf{P}_0$, $\mathbf{P}_1$, and $\mathbf{P}_2$. An alternative picture of the right-hand vertex is that of formation of an isobar of rest mass W, which subsequently decays into a pion plus a nucleon; although somewhat more restrictive, this description should be valid for W in the vicinity of a resonance. For incident energies of 1.35, 2.06, and 2.87 BeV the maximum values of W are 1.52, 1.78, and 2.05 BeV, respectively; hence at the highest incident energy there is the possibility of exciting all four nucleon isobars. It is possible to think of Fig. 2 as giving rise to two independent inelastic proton spectra. The first one being due to protons from the left-hand vertex, which we shall refer to as unexcited protons, has the same peak structure as the π-p total cross section inserted at the right hand vertex (if $\Delta^2>\mu^2$). The second spectrum arising from the right-hand vertex, these protons we shall call decay protons, is expected to be much smoother. One way to see this is to note that observation of $\mathbf{P}_2$ uniquely determines Δ and W, whereas observation of $\mathbf{P}_3$ determines only a range of values for Δ and W. A detailed calculation of the inelastic spectrum based on these assumptions is described in Sec. IV. In Sec. V we compare the results of this calculation with the experimental spectra, and examine both the range of agreement and the systematics of the discrepancies.

II. EXPERIMENTAL DETAILS

1. Beam Geometry and Target Arrangement

The experimental system was designed to measure absolute values of the scattered proton momentum spectrum at a fixed laboratory angle with a momentum resolution of 2% and an angular resolution of 0.5 deg; the lower limit of the momentum range was set at 1 BeV/c. A diagram of the beam layout is shown in Fig. 3. Protons were extracted from the Cosmotron and brought to a focus about 56 ft from the beam exit window by means of three 8-in. aperture quadrupole magnets, $Q1$–$Q3$, as shown in the upper half of the figure. The focal spot was about 2 cm in diameter and the total angular divergence was about 0.5° or less in both the horizontal and vertical planes; these figures vary slightly with the extraction energy. The intensity of the external beam was between 0.5 and 2×10^{10} protons/pulse.

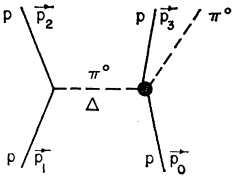

FIG. 2. Feynman diagram for single π^0 production in p-p scattering due to a π^0 exchange.

[15] T. Fujii, G. B. Chadwick, G. B. Collins, P. J. Duke, N. C. Hien, M. A. R. Kemp, and F. Turkot, following paper [Phys. Rev. 128, 1836 (1962)].

A vacuum-insulated liquid-hydrogen target was placed at the focal position. The hydrogen was contained in a stainless steel cylinder 6 in. in diameter, with a length of 14 in. for the 2° and 4° runs and 7 in. for the larger angles; the cylinder was closed with 0.01-in. Mylar windows at either end. The surrounding vacuum tank was provided with large 0.020-in. Mylar windows in the region traversed by the proton beam. The dimensions of the target and windows were such that particles scattered through less than 20° in the horizontal plane passed through only 0.1 g/cm² of Mylar while emerging from the target.

Particles scattered out of the target through a given angle were collimated at a distance of 52 ft from the center of the target by an aperture 2 in. high and 1 in. wide, formed by brass plates 3 ft long, as shown in the lower half of Fig. 1. In order to increase the spatial separation between the scattered protons and the main beam, the unscattered protons were deflected by $M3$ through about 7° towards a steel and concrete beam-stopping enclosure. The scattered protons passed through a field-free region in $M3$, which was created with three concentric tubes of soft iron, and were therefore undeflected by the magnet. The use of this device made it possible to count protons scattered through angles as small as 2° without being faced either with an intolerable background counting rate or with a high level of general radiation in the counting area. The angle of scatter could be varied within the range from 2° to 5° by moving the deflecting magnet $M2$ parallel to the beam direction and readjusting the magnet current accordingly. The actual scattering angle was measured during each run by exposing standard x-ray films to establish the line of the main beam.

Upon leaving the hydrogen target, the scattered particles first passed through a helium-filled bag which extended from the target to the steel shielding wall and then through an evacuated pipe which occupied the space between the shielding wall and the collimator. A vacuum pipe also extended from the analyzing magnets ($M4$ and $M5$) to the counting equipment. For the runs at larger angles (8°, 12°, and 17°) the vacuum pipes were replaced with helium bags to eliminate scattering-in effects from the pipe walls observed in the earlier runs.

2. Momentum Analysis and Detection

The momentum analysis of the scattered particles was effected by a magnetic spectrometer consisting of the two uniform-field bending magnets $M4$ and $M5$. Each magnet bent the central momentum through an angle of 7.5° and was so aligned that the orbit passed symmetrically through the rectangular field region. The momentum calibration of the spectrometer in terms of magnet current was accomplished by means of the floating wire technique to an accuracy of $\pm 0.2\%$; long term regulation of the magnet current was $\pm 0.25\%$.

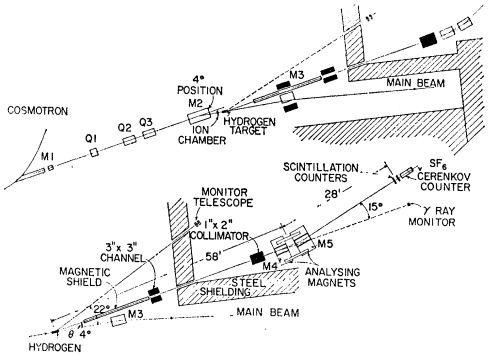

FIG. 3. Experimental arrangement. The upper drawing indicates the over-all trajectory of the beam, starting from the Cosmotron; the lower drawing shows the setup downstream from the target. M refers to bending magnets; Q to quadrupole magnets.

Hysteresis effects in the magnets were measured by the same technique and proved to be less than 0.5% throughout the momentum region of interest. This effect resulted in a small, but detectable, shift between two runs on a given spectrum, one taken with increasing magnet current the other with decreasing current.

After momentum analysis the particles were detected in a simple four-channel scintillation counter hodoscope positioned 25 ft beyond $M5$; the momentum dispersion at the detector was approximately 1.2% per in. Each element of the hodoscope consisted of a rectangular plastic scintillator $1\frac{1}{2}$ in. wide, $4\frac{5}{8}$ in. high, and $\frac{1}{2}$ in. thick connected optically to an RCA 7264 photomultiplier. Each hodoscope channel was formed from two such counters placed one behind the other at a separation of 8 in. The channels were contiguous so that for a given setting of $M4$ and $M5$ a 7.2% momentum range was covered by the four channels. The two central channels were followed by a threshold gas Čerenkov counter[16] in anticoincidence to distinguish between pions and protons. The radiator for this counter was a 3-ft-long column of sulphur hexafluoride gas at room temperature and 215 psi; the Čerenkov light was directed onto the face of a 5-in. photomultiplier (RCA 7046) by means of a 45° mirror. Pions with momenta greater than 1 BeV/c were rejected with an efficiency of 98% or better; protons were below threshold for all energies encountered, but a small fraction were rejected (less than 4%) by virtue of their producing knock-on electrons in the gas and preceding material. The threshold for this process is 1.5 BeV/c; an empirical correction for this effect was readily obtained by looking at the fraction of protons rejected in the regions of momenta above the kinematic limit for pions. The detection scheme did not reject K^+ mesons or deuterons, from the known cross sections for these processes it can be seen that the contamination from these sources will be less than 1% in all regions of observed momentum with the exception

[16] We are indebted to Professor W. Selove and Dr. H. Brody for the use of their counter.

of the contribution from deuteron-plus-single-pion production (see Sec. III).

Pulses from the eight scintillation counters were passed through local limiting and clipping circuits and then to a remote coincidence circuit and scaler system. The resolving time of the coincidence circuits was set at 4 nsec and the scalers had a 10-Mc/sec capability. The coincidence circuits were gated on for a period of 10 msec covering the beam spill-out time of the Cosmotron, typically set at about 7 msec.

3. Spectrometer Calibration

In order to reduce the scaler readings to an abolute momentum spectrum two constants of the spectrometer must be ascertained for each of the four channels: (1) the average momentum of each channel, (2) the acceptance of each channel, $[\Delta\Omega\times(\Delta p)/p]$. The average momentum was accurately obtained from the wire measurements by moving the wire support transversely at the detector. For our geometry and counter size, $\Delta\Omega$ was determined solely by the collimator, hence the variation in acceptance arises from the variation in Δp; the first-order orbit calculations predicted an increase of 11 percent in Δp in going from the lowest to the highest momentum channel. Relative values of $\Delta p/p$ were obtained to an accuracy of $\pm 1\%$ by choosing a smooth region of the measured spectrum and finding empirical normalization factors which brought all four channels into agreement. The absolute values of $\Delta p/p$ were determined by evaluating the slope of the transverse wire measurement curve at the point corresponding to the center of the four channels; using this slope and a counter width of $1\frac{1}{2}$ in. yielded a value for Δp which was assumed to correspond to the average of the four empirical normalization factors. The values of Δp assigned in this way were probably a slight overestimate since any misalignment of the hodoscope counters decreases the effective width; such effects could at most amount to 3%. The variation of $\Delta p/p$ with p for a given channel was shown to be less than a 1% effect by means of careful wire measurements. Assessing all possible errors in the procedure for arriving at $\Delta p/p$ and adding in a 2% allowance for finite-size-source effects, we estimate the total uncertainty in the acceptance of any channel to be $\pm 4.2\%$.

4. Beam Monitoring

The incident proton beam was monitored by two counter telescopes. One viewed the hydrogen target through a lead collimator at an angle of 22° and counted charged particles; the other counted gamma rays emerging from the same collimator as the scattered protons, magnets $M4$ and $M5$ providing a clearing field for charged particles. In addition, a thin-walled, argon filled ionization chamber was placed in front of the target. Owing to beam intensity fluctuations and appreciable recombination effects, the ion chamber was not an adequate relative monitor for normal operation; in the early runs (angle less than 8°) it was employed only as a monitor for background runs where its intensity dependence introduced only a small uncertainty in a rather small (4%) background subtraction. In the later runs it was discarded in favor of the counter telescopes; unlike the ion chamber, the telescope monitors must be recalibrated for the empty target runs. The internal self-consistency of this system of monitors was an assurance that the experimental conditions were remaining constant.

This monitoring system was calibrated in terms of the absolute number of protons passing through the target by measuring the C^{11} activity induced by the beam in a 0.004-in. polyethylene foil. The foil was exposed immediately in front of the target and the C^{11} activity was measured in a NaI well-counter according to the method of Cumming *et al.*[17] These authors quote a cross section of (26.0 ± 1.0) mb for the $C^{12}(p,pn)C^{11}$ reaction over the energy range from 1–3 BeV used in this experiment. The detection efficiency for C^{11} activity was found to be 62% under the conditions of our experiment. This value included an allowance for the loss of C^{11} by diffusion as described by Cumming *et al.*[18]

5. Experimental Procedure

Several runs were made over each spectrum, the criterion for acceptability was reproduction of data within counting statistics. The measured accidental counting rate was less than 1% even for rates of up to 10^5 protons/second, rates reached only in the momentum region of the elastic peak. Effects of scaler dead time, which were also apparent only in this interval, were eliminated by running with reduced intensity of the incident beam. A background run was taken for each spectrum by emptying the hydrogen target. In the inelastic part of the spectrum the background was always about 4% of the target full rate; however, in the region of the elastic peak especially at the smaller angles the background was as high as 10% owing to the diffraction scattering from the carbon nuclei in the target windows. Normally four foil calibrations were made at each energy and angle, three with the target full and one with it empty.

III. EXPERIMENTAL RESULTS

1. Cross-Section Calculation

The relationship between the differential cross section and the quantities measured in the experiment is given by the equation:

$$\frac{d^2\sigma}{d\Omega dp}(\theta,p)=\frac{N(\theta,p)/p}{N_I\rho_H t N_0\Delta\Omega(\theta)\Delta p/p}. \tag{3.1}$$

[17] J. B. Cumming, G. Friedlander, and C. Swartz, Phys. Rev. **111**, 1368 (1958).

[18] J. B. Cumming, A. M. Poskanzer, and J. Hudis, Phys. Rev. Letters **6**, 484 (1961).

The quantities in this equation are defined in the following way: A particle emerging from the target with a momentum p and at a scattering angle θ follows a trajectory which passes through the center of the collimator, traverses the spectrometer symmetrically, and reaches the center of one of the four channels. For any particular run, $N(\theta,p)$ is the total number of protons counted in one of the channels and N_I is the corresponding number of incident protons. The number of hydrogen nuclei per cm^2 in the target is given by $\rho_H t N_0$, where ρ_H is the density of liquid hydrogen, t is the effective length of the targer, and N_0 is Avogadro's number. The solid angle $\Delta\Omega$ is defined by the back aperture of the collimator, and the fractional momentum width $\Delta p/p$ for each channel was determined by the method described in the preceding section.

In obtaining the simplified formula of Eq. (3.1) for the cross section, the following approximations were used. Because of the small extent of the collimator (1 in.×2 in.) in comparison with its distance from the target (52 ft), (i) the scattering angle θ is independent of the azimuthal angle, and (ii) the solid angle $\Delta\Omega$ is constant to first order over the range of momentum Δp, defined by the spectrometer and the counter telescopes. There were no shadow effects from the magnet pole pieces since the 6-in. gap was much larger than the vertical extent of the collimator aperture (2 in.). In addition, the vertical dimension of the counters ($4\frac{5}{8}$ in.) was sufficient to encompass the vertical beam size, even if one ignores the assistance afforded by the vertical focusing of the spectrometer magnet.

The number of incident protons N_I was related to the monitor counts M by Eq. (3.2), in which N_f is the number of protons recorded in the appropriate foil measurement and M_I the monitor counts corresponding to N_f.

$$N_I=(N_f/M_f)M. \tag{3.2}$$

The value of N_f was obtained from the measured activity of an irradiated polyethylene foil by Eq. (3.3).

$$N_f=\frac{C_f W}{\epsilon\sigma N_0 S}\times\frac{\lambda t_1\exp[\lambda(t_2-t_1)]}{[1-\exp(-\lambda t_1)]\{1-\exp[-\lambda(t_3-t_2)]\}}, \tag{3.3}$$

where λ=decay constant of C^{11}, W=molecular weight of CH_2, S=foil thickness in g/cm^2, ϵ=detection efficiency of foil counting. σ=cross section for the reaction $C^{12}(p,pn)C^{11}$, C_f=number of C^{11} counts recorded, t_1=time at which irradiation ceased (starting time of irradiation $t_0=0$), t_2=starting time of counting period, and t_3=end of counting period. In general, S was $8.5-9.5\times10^{-3}$ g/cm^2, t_1 varied from 2 to 5 min, (t_2-t_1) was about 10 min, and (t_3-t_2) was 5 min. In order to minimize systematic effects, most of the foils were counted two or three times at different stages of their decay. The values of constants which were used to obtain the absolute values of the cross sections are listed in Table I.

TABLE I. Values of constant factors.

Constant	Value
ρ_H	0.07 g/cm^3
t	14.92±0.05 in. for 2°, 3°, and 4° 7.90±0.05 in. for 8°, 12°, and 17°
$\Delta\Omega$	5.16×10^{-6} sr for 2°, 3°, and 4° 5.58×10^{-6} sr for 8° 5.17×10^{-6} sr for 12° 5.32×10^{-6} sr for 17°
$(\Delta p/p)$[a]	0.0176 for 2°, 3°, and 4° 0.0179 for 8° 0.0192 for 12° 0.0159 for 17°
λ	0.03397 min^{-1}
W	14.03 g
ϵ	0.62
σ	26.0±1.0 mb

[a] Average value of the four channels.

TABLE II. Incident proton energies and scattering angles.

Nominal beam energy (BeV)	True beam energy (BeV)	Scattering angle (deg)
1.35	1.335±0.005	2.37±0.27[a]
	1.351±0.005	3.38±0.27
	1.384±0.005	4.30±0.27
	1.346±0.006	8.12±0.28
	1.346±0.006	12.03±0.29
	1.337±0.006	17.35±0.30
2.1	2.064±0.006	2.74±0.27
	2.096±0.006	4.17±0.27
	2.066±0.007	8.43±0.28
	2.065±0.008	12.00±0.29
	2.081±0.009	17.33±0.30
2.9	2.868±0.009	2.72±0.27
	2.867±0.009	4.51±0.27
	2.869±0.010	8.53±0.28
	2.858±0.010	12.17±0.29
	2.897±0.013	17.75±0.30

[a] Spread due to the angular divergence of the incident beam and the finite size of the scattering source.

The counts with the target empty, which were mainly due to scattering from the Mylar window of the target, have been subtracted from those with the target full before calculating the cross sections. A correction was made where necessary for pion contamination, using the number of triple coincidence counts between the telescope and the Čerenkov counter; however, pions were excluded on kinematic grounds over a considerable fraction of the momentum range at all incident energies. For instance, the maximum pion momenta at 4° are 1.10, 1.74, and 2.54 BeV/c for the incident energy of 1.35, 2.1, and 2.9 BeV, respectively.

Table II gives a list of the incident beam energies and the corresponding angles at which the proton spectra were measured. The true beam energy was calculated from the position of the elastic peak in the measured spectrum and the scattering angle. The quoted error

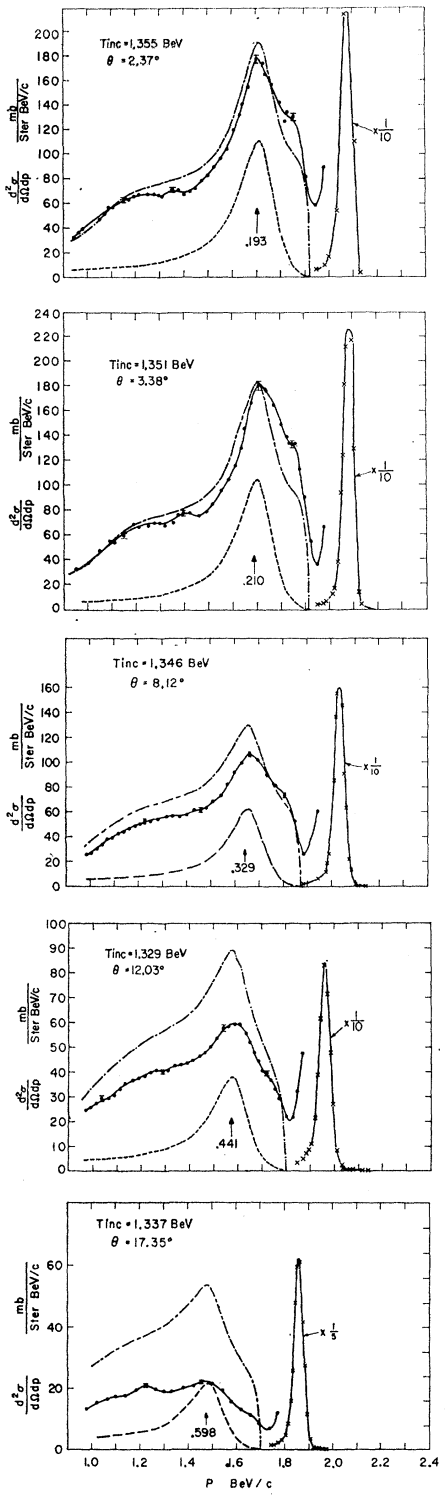

FIG. 4. Laboratory differential cross sections of secondary protons at a nominal incident proton kinetic energy of 1.3 BeV, and various laboratory angles. Absolute errors are ±6–7%; errors are statistical. — — — Theoretical: unexcited proton. —·—·— Theoretical: unexcited proton+decay proton. For explanation of arrow, see text.

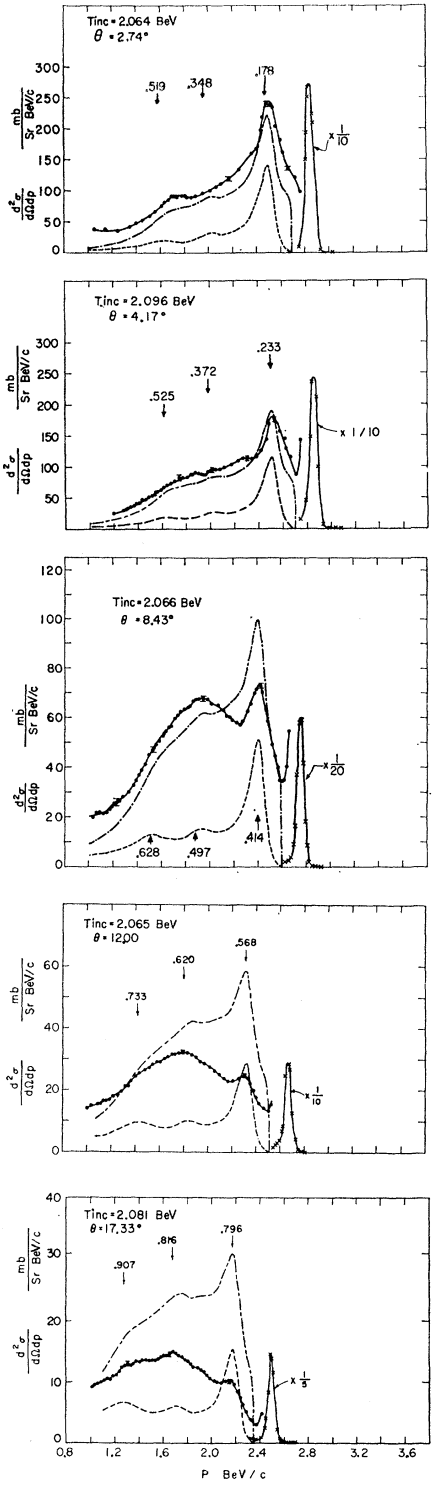

FIG. 5. Laboratory differential cross sections of secondary protons at a nominal incident proton kinetic energy of 2.1 BeV, and various laboratory angles. Absolute errors are ±6–7%; errors shown are statistical. — — — Theoretical: unexcited proton. —·—·— Theoretical: unexcited proton+decay proton. For explanation of arrow, see text.

of each energy includes the uncertainty in locating the elastic peak (± 3 MeV/c) and the error in determination of the mean angle ($\pm 0.1°$).

The standard deviation of the relative cross sections over a given run as determined by counting statistics was about 1.0% in the region of the elastic peak, about 1.5% in the region occupied by the prominent peak in the inelastic spectrum, and 2 to 4% over the rest of the momentum range. Since the spectrum at each energy and angle was measured at least twice and each step of the spectrometer setting was small enough to allow the momentum width of different channels to overlap each other, there were several independent measurements of the cross sections at a given value of p. The reproducibility of the values among these independent measurements was compatible with the counting statistics. In the graphical presentation of the spectra (Figs. 4–6) each plotted point is actually the average of three or four experimental pionts which fell in the same 2% momentum bin.

The principal sources of error in converting the cross sections into absolute values were the uncertainties in the cross section for the production of C^{11} and in the determination of the absolute value of $\Delta p/p$. The former amounts to $\pm 4\%$ according to Cumming *et al.*[17] and the latter to $\pm 4.2\%$ as discussed in the preceding section. These figures were combined with those introduced by counting statistics and small uncertainties in other constants to give values ranging from ± 6.5 to $\pm 7.2\%$ over the entire range of the measurement.

2. Salient Features of the Data

The experimental differential cross sections, obtained in the manner described above, are presented in Figs. 4–6 for the incident energy 1.35, 2.1, and 2.9 BeV, respectively. They show the experimental quantity $d^2\sigma/d\Omega dp$ as a function of the proton momentum for various laboratory angles. It is convenient to discuss some of the features of the inelastic spectra in terms of isobar production. If the interaction is assumed to proceed through the sequence

$$p+p \rightarrow N+N^* \searrow N+\pi\text{'s}, \qquad (3.4)$$

the momentum of the unexcited proton recoiling from the isobar N^* is determined by kinematics for any particular mass W of N^*. The momenta of unexcited protons recoiling from the isobars of 1.23, 1.52, 1.69, and 1.92 BeV, corresponding to known maxima in the π-p cross sections, are indicated by arrows in the figures.

The unexcited proton peak from the 3, 3 (1.23-BeV) isobar is present at every angle for all three incident energies. It is particularly prominent at small angles.

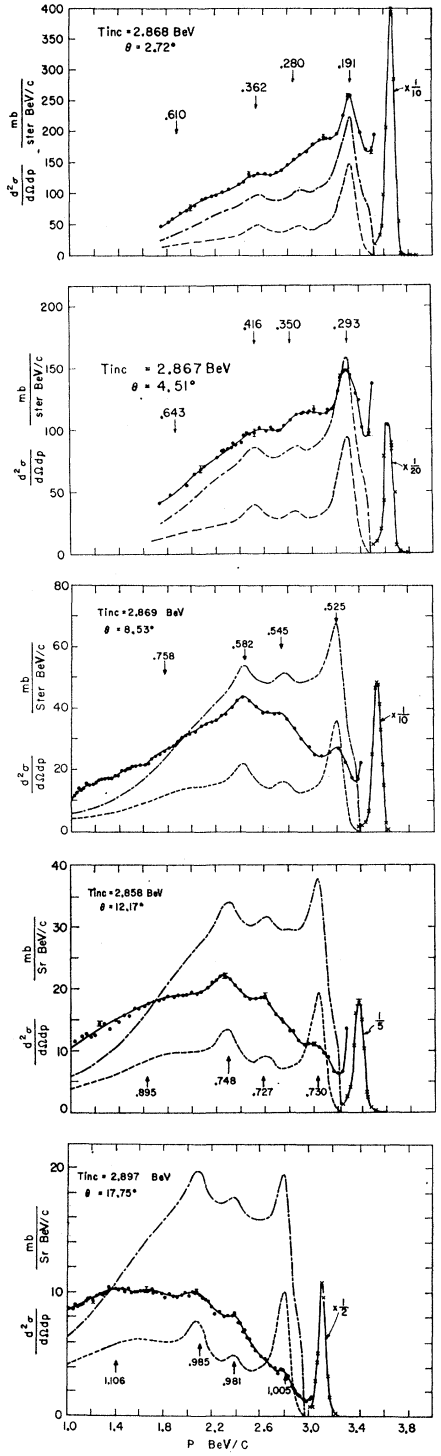

FIG. 6. Laboratory differential cross-sections of secondary protons at a nominal incident proton kinetic energy of 2.9 BeV, and various laboratory angles. Absolute errors are ±6–7%; errors shown are statistical. — — — Theoretical: unexcited proton. —·—·— Theoretical: unexcited proton+decay proton. For explanation of arrow, see text.

However, there is a very marked decrease in magnitude as the angle, consequently the four-momentum transfer to the unexcited nucleon, increases. One also observes the appearance of a shoulder on the high momentum side of the 3, 3 peak, especially at small angles at 1.35 BeV.

Consider the 1.35-BeV data. Since this energy corresponds to the threshold for producing the 1.52-BeV isobar, the momentum of the unexcited nucleon (0.75 BeV/c) is too low for this experiment to record. There is some evidence for fine structure below the 3, 3 peak. Although our detection scheme did not exclude deuterons, only the small peak at 1.2 BeV/c in Fig. 4(e) is consistent with deuterons from the process $p+p \rightarrow d+\pi^+$.

At 2.1 BeV it is possible to excite the 1.23-, 1.52-, and 1.69-BeV isobars. In addition to the prominent 3, 3 peak already mentioned, there is some evidence for the 1.52-BeV isobar especially at the angles larger than 4°, but no structure readily identifiable with the 1.69-BeV isobar.

At 2.9-BeV incident energy, it is possible to excite all four isobars. Peaks corresponding to unexcited protons from the 1.52- and 1.69-BeV isobars can now be clearly discerned, particularly at 8°, 12°, and 17°. There is, however, no evidence for a peak corresponding to formation of the 1.92-BeV isobar.

One notable feature common to both 2.1- and 2.9-BeV data is the gross behavior with increasing angle of the inelastic spectrum below the 3, 3 peak; the character changes from one monotonically increasing with momentum at the small angles, to one with a broad peak about midscale at large angles.

In summary, it can be said that:

(a) Intense peaks corresponding to the 3, 3 isobars are observed at all energies, the intensity decreases rapidly with increasing angle of scattering.

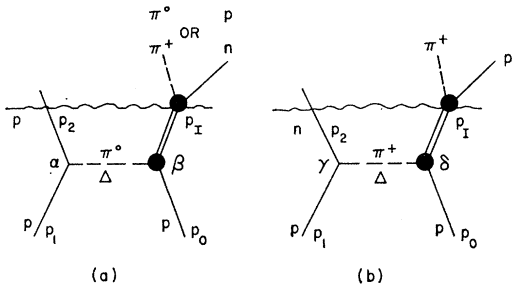

FIG. 7. Feynman diagrams for single pion production in pp scattering (a) by a π^0 exchange; (b) by a π^+ exchange. Proton (neutron) is denoted by $p(n)$, while the isobar is represented by a double line. Subscripted p's represent four-momenta; Δ is the four-momentum of the virtual pion. α, β, γ, δ label the vertices. The wavy lines separate the isobar production and decay, which are assumed to be independent processes. The proton which is produced together with the isobar, or excited nucleon, is referred to as the unexcited proton, in contrast to the decay proton from the isobar.

(b) Peaks corresponding to the 1.52- and 1.69-BeV isobars are also observed, particularly at 2.9-BeV incident energy and at the larger angles.

(c) No peak corresponding to the 1.92-BeV isobar is observed.

(d) A shoulder on the high-momentum side of the 3, 3 peak is observed.

(e) There still remains some fine structure not readily identifiable with any known isobar.

In a later section, interpretation of the spectra will be discussed in terms of the OPE model.

IV. CALCULATION OF THEORETICAL SPECTRA

1. The One-Pion Exchange Model

While the isobar model predicts the appearance of peaks in the experimental spectra corresponding to the formation of isobars, a more specific mechanism for isobar production is needed to account for the sharp decrease of the differential cross sections with increasing angles at a fixed incident energy. Such a mechanism, favoring low momentum transfers, is provided by the OPE model.

For the purpose of this calculation we shall interpret the OPE model to mean that inelastic p-p collisions proceed in the following way:

(a) excitation of a single isobar through a peripheral collision mediated by one-pion exchange between the colliding particles;

(b) decay of the isobar into a nucleon and one pion, i.e., we confine ourselves to single pion production.

This two-step process is represented by the Feynman diagrams of Fig. 7. The wavy lines separate the isobar production and decay, which are considered to be different processes. The vertices are labeled, α, β, γ, and δ. In the production process, the symbols p with a subscript represent the four-momenta, while Δ is the four-momentum of the virtual pion. The letter p (n) indicates a proton (neutron). The proton which is produced together with the isobar is referred to as the unexcited proton, in contrast to the decay proton from the isobar.

It must be stated that on the basis of OPE model, calculations can be made with two nucleons and a pion in the final state independently of the assumption of isobar formation. The latter is nevertheless retained for the following reasons:

(a) The use of the isobar concept in the calculation is equivalent to neglecting diagrams in which final state nucleons are interchanged, as well as all interference terms except that resulting from the exchange of initial nucleons. The unimportance of these omitted terms has been shown by DaPrato.[19]

(b) It is justifiable to speak of an isobar when the pion-nucleon system has a resonance which dominates the

[19] G. DaPrato, Nuovo cimento **22**, 123 (1961).

interaction in the region of the resonance energy, as is the case at the 3, 3 resonance.

To compare the predictions of the model with the experimental results, we must calculate the differential cross section of the unexcited proton given by diagram 7(a), as well as that of the decay proton present in both diagrams. The inelastic proton spectrum is then given by the sum of the unexcited proton and the decay proton spectra, without the interference terms, as stated above.

2. Unexcited Proton Spectrum

From a formula given by Selleri[13] (with correct normalization) we can readily obtain the laboratory differential cross section with respect to angle and momentum for unexcited protons:

$$\frac{d^2\sigma}{d\Omega_2 dp_2}=\frac{f^2m}{\pi^2\mu^2}\frac{p_2^2}{p_1E_2}R(W)\sigma(W)\times[a(T_2)+b(T_2,W)+c(T_2,W)], \quad (4.1)$$

where f^2=pion-nucleon coupling constant=0.08, m=nucleon mass, and μ=pion mass; p_1, T_1, E_1=laboratory momentum, kinetic energy, and total energy of the incident proton, respectively; W=total energy of π and p in their center-of-mass system:

$$W=[(E_1+m-E_2)^2-(p_1^2+p_2^2-2p_1p_2\cos\theta_2)]^{1/2}; \quad (4.2)$$

θ=lab angle of unexcited proton; p_2, T_2, E_2=laboratory momentum, kinetic energy, total energy of unexcited proton, respectively;

$$R(W)=\tfrac{1}{2}[W^4-2W^2(m^2+\mu^2)+(m^2-\mu^2)^2]^{1/2};$$

$\sigma(W)=\pi p$ total cross section at a center-of-mass energy W;

$$a(T_2)=\Delta_2^2/(\Delta_2^2+\mu^2)^2;$$

$$b(T_2,W)=\Delta_1^2/(\Delta_1^2+\mu^2)^2;$$

$$c(T_2,W)=\phi/(\Delta_1^2+\mu^2)(\Delta_2^2+\mu^2),$$

$$\phi=(W-m)[(E'_{p_0}+m)(E'_{p_1}+m)]^{1/2}\cos\theta_i+(W+m)[(E'_{p_0}-m)(E'_{p_1}-m)]^{1/2}(3\cos^2\theta_i-1)/2;$$

$E'_{p_{1,0}}=(W^2+m^2+\Delta_{2,1}^2)/2W$=energy of proton 1, 0 in the πp center-of-mass system-θ_i=angle between protons 0 and 1 in the πp center-of-mass system·

$$\cos\theta_i=\left[\frac{1}{4W^2}(2\alpha-\Delta_1^2)(2\alpha-\Delta_2^2)-\alpha\right]\times[(E'_{p_1}{}^2-m^2)(E'_{p_0}{}^2-m^2)]^{-1/2},$$

$$\Delta_1^2=m^2+2m(T_1-T_2)-W^2=(P_2-P_1)^2, \quad (4.3)$$

$$\Delta_2^2=2mT_2=(P_2-P_0)^2, \quad (4.4)$$

where $\alpha=m(T_1+m)$, and P represents the four-momentum.

The assumptions underlying formula (4.1) are

(a) The pionic form factor of the nucleon is taken to be independent of Δ and equal to unity.

(b) The pion propagator is taken to be $1/(\Delta^2+\mu^2)$, neglecting higher order renormalization effects.

(c) The virtuality of the pion is ignored, with the consequence that vertices β and δ are given by the phenomenological cross section $\sigma(W)$ for pions on the mass shell.

Formula (4.1) can be understood in the following way. Apart from factors due to the incident flux and the phase space, the cross section for diagram 7(b) is given by the square of the matrix element $M(P_1,P_0)$ which is proportional to $\{fu(P_2)\gamma_5 u(P_1)/[(P_2-P_1)^2+\mu^2]\}\sigma(W)$. For the moment we do not consider the identity of the protons. The term σ is the contribution of vertex δ, assuming that the pion is real. The other term in the numerator is the well-known γ_5 coupling for vertex γ (the u's are nucleon spinors), while the denominator is the pion propagator. When M is squared, summed over spins in the final state, and averaged over spins in the initial state, we obtain a factor proportional to $f^2\sigma(W)b(T)$. Because we have two protons in the initial state, the Pauli principle prescribes $M_{\text{total}}=M(P_1,P_0)-M(P_0,P_1)$. This gives rise to three terms in the cross section a, b, and c, where c represents the interference term.

These terms show the decrease of the differential cross section with increasing momentum transfer. As seen in Eqs. (4.3) and (4.4), Δ_1^2 and Δ_2^2, hence a, and b display opposite behavior as a function T_2. For the high-momentum branch of the unexcited spectrum the b term dominates; its effect is compensated however by $R(W)$ which, being essentially a phase space factor, decreases monotonically as p_2 increases, and vanishes at the upper limit of the inelastic spectrum.

The shape of the differential cross section is governed by that of the $\pi^{\pm}p$ cross section since $\sigma_{\pi^0 p}$ is $\frac{1}{2}(\sigma_{\pi^+ p}+\sigma_{\pi^- p})$ from simple isotopic spin considerations; hence peaks corresponding to the $\pi^{\pm}p$ resonances are expected to appear in the inelastic spectrum.

The above features are illustrated in Fig. 9, where the 3, 3 peak is prominently displayed for the calculated spectrum at 1.35 BeV and 2.37°.

3. Decay Proton Spectrum

In addition to the pole approximations already stated, an angular distribution for the decay proton must be assumed. For simplicity, we assume that the isobar decays isotropically in its own rest system. The data of Fickinger *et al.*[14] lend some support to this assumption; although the angular distribution of the decay proton shows some anisotropy for events in the 3, 3 resonance region, this anisotropy will be reduced when an average is taken over the isobar production angles. A more rigorous application of the OPE model which obviates this

assumption would have been to insert the π-p differential cross section at vertices β and δ of Fig. 7 rather than the total cross section.

The decay proton differential cross section with respect to solid angle Ω and energy E in the over-all barycentric system is given by

$$\frac{d^2\sigma}{d\Omega dE}=\int_{W_{\min}^2(E)}^{W_{\max}^2(E)}\int_0^{2\pi}\frac{d^2\sigma(\xi,\phi,W)}{d\Omega_I dW^2}\times\frac{1}{4\pi}\left(\frac{\partial\Omega^*}{\partial\Omega}\right)_{E,W,\phi}\left(\frac{\partial\cos\xi}{dE}\right)d\phi dW^2, \quad (4.5)$$

where the angles specifying the kinematics of the decay process are shown in Fig. 8. The first factor in the integrand gives the differential cross section for isobar production in the element of solid angle $\Delta\Omega_I(\xi,\phi)$, with a squared mass between W^2 and W^2+dW^2. This is readily obtained from the unexcited proton cross section by means of a simple Jacobian transformation, noting that for isobar production the intermediate pion can be a π^+ giving $\pi^+p\rightarrow\pi^+p$ at the four-particle vertex, as well as a π^0 giving $\pi^0p\rightarrow\pi^0p$ (and also $\pi^0p\rightarrow\pi^+n$, but this is discarded since only protons are detected). The term $(1/4\pi)(\partial\Omega^*/\partial\Omega)$ gives the transformation of the isotropic angular distribution of the decay proton in the isobar rest system (denoted by the asterisk) to the angular distribution in the over-all barycentric system.

Equation (4.5) can be rewritten as

$$\frac{d^2\sigma}{d\Omega dE}=\frac{f^2m^2}{8\pi^3\mu^2}\frac{1}{p_0E_0^2}\int_{W_{\min}^2(E)}^{W_{\max}^2(E)}\int_0^{2\pi}\times[a+b+c]W^2\sigma(W)d\phi dW^2, \quad (4.6)$$

where a, b, and c have the same form as before, but now referred to isobar variables;

$p_0(E)_0$ = momentum (energy of the incident proton in over-all barycentric system;

$$\sigma(W)=2\sigma_{\pi^+p\rightarrow\pi^+p}+\sigma_{\pi^0p\rightarrow\pi^0p}$$
$$=\tfrac{5}{2}\sigma_{\pi^+p\rightarrow\pi^+p}+\sigma_{\pi^-p\rightarrow\pi^-p}-\tfrac{1}{2}(\sigma_{\pi^-p\rightarrow\pi^-p}+\sigma_{\pi^-p\rightarrow\pi^0n})$$

The integration was performed numerically with a IBM 7090 computer, the ϕ integration at intervals of 5 deg, and the W integration at intervals of $\sim$5 MeV. The laboratory differential cross section $d^2\sigma/d\Omega_{\rm lab}dp_{\rm lab}$ is readily obtained by multiplying (4.6) with the transformation factor $p^2_{\rm lab}/p_{\rm c.m.}E_{\rm lab}$.

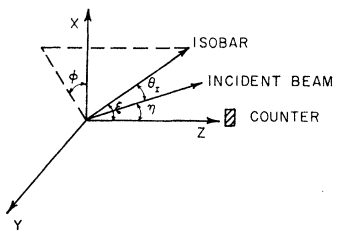

FIG. 8. Coordinate system for isobar decay. The counter direction is taken to be the polar axis. ξ, ϕ are the polar and azimuthal angles of the isobar, η is the angle of the incident beam. θ_I is the angle between the isobar and the incident beam direction. All angles are referred to the over-all center-of-mass system.

The values of σ_{π^+p} and σ_{π^-p} used for the decay and recoil spectra are taken from the data collected by Noyes and Edwards[20] up to 450-MeV incident-pion lab kinetic energy, and those of Devlin *et al.*,[21] Brisson *et al.*,[22] and Longo *et al.*[23] beyond 450 MeV. The partial cross sections $\sigma_{\pi^+p\rightarrow\pi^+p}$ and $\sigma_{\pi^-p\rightarrow\pi^-p}$ are taken from various sources.[24] The uncertainties in the quoted cross sections vary between 5–10%.

In formula (4.6), $\sigma(W)$ is dominated by the π^+p elastic cross section, and therefore exhibits the characteristic 3, 3 resonance at an isobar mass of $\sim$1.23 BeV. As in the unexcited proton spectrum, the terms a, b, c display the prominence of isobar production with low momentum transfers. Because of the averaging integration, no striking structure is obtained in the decay spectrum. A typical decay spectrum is shown in Fig. 9.

V. DISCUSSION

The results of the calculation described in the preceding section are displayed along with the experimental data in Figs. 4–6; in each graph the lower curve gives the unexcited spectrum; the upper curve gives the sum of unexcited plus decay spectra. The numbers accompanying the arrows indicating the predicted locations of the isobar peaks are the smaller of the two possible four-momentum transfers, Δ_1, of Eq. (4.3), expressed in BeV/c. In comparing the theoretical and experimental curves it is important to recall the following facts: (a) The calculation of the unexcited proton spectrum includes all possible OPE channels which yield inelastic protons. (b) The decay calculation includes only the contribution coming from single-pion production. (c) At 1.35 BeV, two-pion production in a p-p collision is probably less than 10% of single production,[25] while at 2.0 and 2.9 BeV multi-pion production is about 60–80% of single production.[4–7] (d) The kinematic limit for protons from two-pion production lies at a momentum slightly above the 3, 3 isobar peak, about 20–25 MeV/c higher throughout our experimental range.

The agreement, both in amplitude and in shape, of OPE curves and the experimental data at 2° and 4° at

[20] H. P. Noyes and D. N. Edwards, Phys. Rev. **118**, 1409 (1960).
[21] T. J. Devlin, B. J. Moyer, V. Perez-Mendez, Phys. Rev. **125**, 690 (1962).
[22] J. C. Brisson, J. Detoeuf, P. Falk-Variant, L. Van Rossum, G. Valladas, and L. C. L. Yuan, Nuovo cimento **19**, 210 (1961).
[23] M. J. Longo and B. J. Moyer, Phys. Rev. **125**, 701 (1962).
[24] P. Falk-Variant and G. Valladas, Revs. Modern Phys. **33**, 362 (1961); V. G. Zinov and S. M. Korenchenko, Soviet Phys.—JETP **11**, 794 (1960); L. Bertanza, R. Carrara, A. Drago, P. Franzini, I. Manelli, G. V. Silverstrini, and P. H. Stoker, Nuovo cimento **19**, 467 (1961); F. Grard, G. Macleod, L. Montanet, M. Cresti, R. Barloutaud, C. Choquet, J. M. Gaillard, J. Heughebaert, A. Leveque, P. Lehmann, J. Meyer, and D. Revel, *ibid.* **22**, 193 (1961).
[25] E. L. Hart (private communication).

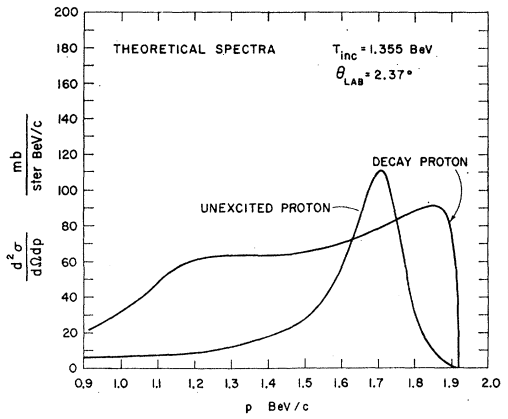

FIG. 9. Typical calculated spectra of inelastic protons. The peak in the unexcited proton spectrum is due to the (3/2, 3/2) resonance in π-p scattering.

1.35 BeV is quite remarkable; the absolute agreement is perhaps better than would be anticiapted in view of the experimental uncertainties, viz., the $\pm 7\%$ in our absolute cross section scale and a comparable uncertainty in the π-p cross section data used in the OPE calculation. The theory nicely predicts the shoulder appearing on the high-momentum side of the 3, 3 peak; this effect is caused by the steeply rising decay spectrum. There is, however, a noticeable discrepancy at the shoulder; part of this discrepancy may be experimental, being attributable to the tail of the huge elastic scattering peak. For the 8° and 12° data at 1.35 BeV the agreement in shape is still rather good, but the theory overestimates everywhere by a constant factor of 1.2 and 1.5, respectively. Finally, at 17°, the overestimate is a factor of 2 at the low-momentum end and significantly larger at the 3, 3 peak.

Proceeding to higher incident energies one observes that the agreement at 2° and 4°, although somewhat poorer than at 1.35 BeV, is still surprisingly good; a tendency for the theory to underestimate at the smallest angle is discernible. However, for the angles greater than 8° at 2.1 BeV and greater than 4° and 2.9 BeV the agreement both in amplitude and in shape gets progressively worse, until at 17° the similarity is nearly unrecognizable and the OPE theory is too large by a factor of 5 at the 3, 3 isobar peak. At large angles the theoretical curves also lie high throughout most of the momentum range below the 3, 3 peak, the region where one would naively expect the theory to be low because of the large contribution from multipion production. The gross discrepancies observed are clearly related to momentum transfer.

The simplest way to study the deviations from the OPE theory is to concentrate on the unexcited part of the inelastic spectrum; as can be seen from Eqs. (4.1) and (4.6) the unexcited cross section is a function of a unique Δ_1^2, whereas the decay cross section involves an integration over a considerable range of Δ_1^2. We further limit ourselves to the single-pion production region of the spectrum, i.e., the 3, 3 isobar peak; although the double production "threshold" is essentially at the peak, we expect a negligible contribution from this source as previous bubble chamber experiments[5,7] show a slowly rising inelastic proton spectrum due to two-pion production. In order to extract the unexcited cross section from the experimental spectra it is necessary to adopt a somewhat arbitrary but reasonable procedure, we assume

$$\sigma_{U,E}=\sigma_{\text{total},E}\frac{\sigma_{U,T}}{\sigma_{U,T}+\sigma_{D,T}}, \tag{5.1}$$

with

$$\sigma=d^2\sigma/d\Omega dp,$$

and subscripts have the meanings: E=experiment, T=theory, U=unexcited, D=decay. The use of Eq. (5.1) in the region where the OPE theory and experiment are in agreement is a matter of consistency; however, its use for large Δ_1^2 where theory and experiment strongly disagree is equivalent to the additional assumption that at the 3, 3 peak both $\sigma_{U,T}$ and $\sigma_{D,T}$ deviate from reality by the same factor. Since $\sigma_{U,T}$ has a somewhat steeper θ dependence than $\sigma_{D,T}$, formulas (5.1) may tend to overestimate $\sigma_{U,E}$ at large Δ_1^2. In Fig. 10 we have plotted the unexcited c.m. angular distribution at the 3, 3 peak obtained by this procedure for the three incident energies; the broken curve is the predic-

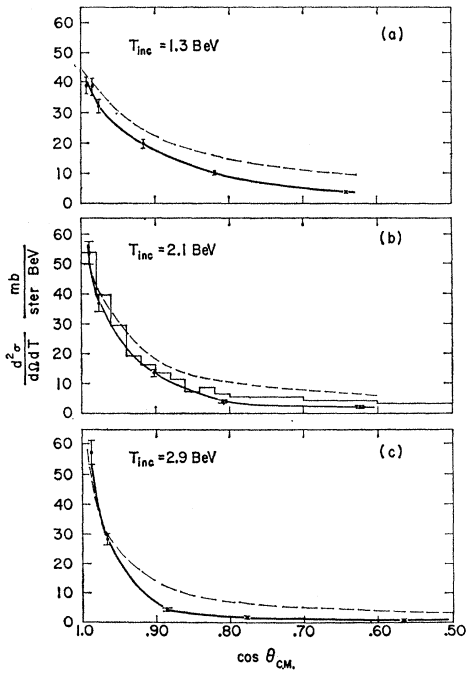

FIG. 10. Center of mass angular distribution of unexcited protons at the (3,3) peak, given by the extraction procedure discussed in the text. The dashed lines are predictions of the OPE model. In (b), the histogram represents the neutron angular distribution obtained by Fickinger *et al.* (reference 14), normalized to the present data.

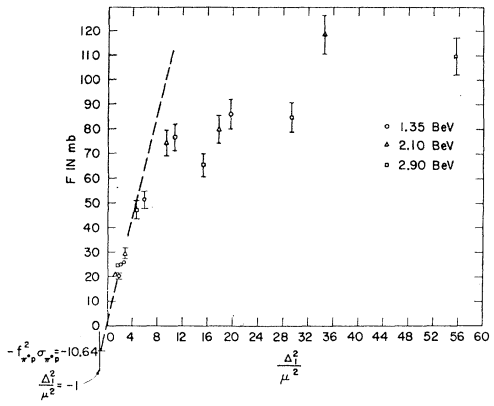

FIG. 11. Chew-Low plot of $\sigma_{U,E}$ evaluated at the 3, 3 isobar peak; F is defined in Eq. (5.2) of the text. The dashed line is the asymptotic OPE prediction.

tion of the OPE theory. In the 2.1-BeV graph, we have also plotted the relative angular distribution of all neutrons coming from the reaction $p+p \rightarrow p+n+\pi^+$ at 2 BeV as observed by Fickinger *et al.*[4]; their data is consistent with the prediction that the neutron is nearly always the unexcited nucleon. The agreement between the two experimental curves lends support to our method of obtaining the unexcited cross section.

One method for exhibiting the departure of the data from the OPE prediction as a function of momentum transfer is afforded by the Chew-Low extrapolation procedure.[9] By a rearrangement of Eq. (4.1) one obtains the extrapolation form

$$F \equiv \frac{\pi^2 p_1 E_2}{m p_2^2} \frac{\Delta_1^2}{R[a+b+c]} \sigma_{U,E} \sim f^2 \sigma_{\pi P}(W) \frac{\Delta_1^2}{\mu^2}, \quad (5.2)$$

where $\sigma_{U,T}$ has now been replaced by $\sigma_{U,E}$. The Chew-Low plot for the 3, 3 isobar at the three incident energies is shown in Fig. 11, in which the left-hand side of Eq. (5.2) is plotted against Δ_1^2; the straight line is a plot of the right-hand side of Eq. (5.2). The errors indicated on the points are experimental only, they do not include the unknown uncertainty involved in the use of Eq. (5.1) to obtain $\sigma_{U,E}$. From this graph one observes that the experimental points agree with the OPE theory to within $\pm 15\%$ out to $\Delta_1^2 = 6\,\mu^2$; at larger Δ_1^2 the points fall progressively lower until at $55\,\mu^2$ they are about a factor of 5 below the prediction. It also appears that to within $\pm 20\%$ the deviation from the OPE theory is a function of Δ_1^2 alone, i.e., insensitive to the incoming energy in the region 1.3 to 2.9 BeV.

In view of the factor of two suppression at $\Delta_1^2 = 16\,\mu^2$ seen in Fig. 11, it may seem puzzling that the agreement is so good for the total inelastic cross section at 1.35 BeV and small angles [Figs. 4(a), (b)] in the momentum region near 1 BeV/c where Δ_1^2 is $\sim 16\,\mu^2$. The reason for this is that the unexcited cross section is only a small fraction of the total at this momentum; the decay cross section—the main contributor—arises from much smaller values of Δ_1^2 where the production cross section agrees with predictions. This same effect also helps to explain the relatively good agreement obtained at the higher energies at small angles; an additional factor aiding the agreement there is that the angular distribution of the nucleons from single-pion production is more peaked forward than that for multiple production.[4–7]

Recently, Ferrari and Selleri[26] have proposed an extension of the OPE model in which they suggest that the OPE term completely dominates single-pion production in nucleon-nucleon collisions, even for momentum transfers as large as $50\,\mu^2$. The experimental test proposed for this hypothesis is that a function, $\Gamma(\Delta_1^2)$, should exist which brings the predictions of the simple OPE theory into agreement with experimental cross sections at all incident energies. These authors obtained $\Gamma(\Delta_1^2)$ by assuming it had the functional form,

$$\Gamma_{\text{F.S.}}(\Delta_1^2) = \frac{1}{1+(\Delta_1^2+\mu^2)/\alpha}. \quad (5.3)$$

They determined the parameter α to be $\sim 60\,\mu^2$ by fitting the single-production total cross sections for p-p collisions at 0.97 and 2.85 BeV. In a theoretical analysis they showed that $\Gamma(\Delta_1^2)$ is composed of two factors: (a) an off-mass-shell correction to the π-p scattering, and (b) a pionic form factor of the nucleon multiplied by a correction to the pion propagator. By calculating the first factor in the 3, 3 resonance region, they were able to extract an empirical form factor. Thus, in this picture it is the pionic form factor which suppresses the prediction of the OPE model for large Δ_1^2.

In Fig. 12 we have plotted the ratio $\sigma_{U,E}/\sigma_{U,T}$ against Δ_1^2, again evaluated at the 3, 3 isobar peak and for all three incident energies. This ratio is precisely[27] $\Gamma^2(\Delta_1^2)$—assuming it exists—and as previously noted in connection with the Chew-Low plot, appears to be independent of incoming energy within limits. The dashed curve in Fig. 12 is $\Gamma_{\text{F.S.}}^2(\Delta_1^2)$ obtained by Ferrari and Selleri in the manner mentioned above; the present method is more direct in that no particular functional form is assumed. In view of the differences between the two methods, a point by point agreement between the two curves is not expected. A precise comparison can be made only after performing a certain integration over Δ_1^2; in this sense the agreement between the two curves is acceptable. It is noted that our ratio becomes larger than one at $\Delta^2 = 2\mu^2$, (the function $\Gamma_{\text{F.S.}}^2(\Delta_1^2)$ cannot have this behavior because of the form imposed); this is a reflection of the fact that at the smallest angle in Figs. 5 and 6 the experimental data lie above the OPE curve at the 3, 3 peak for the case of 2.1 and 2.9 BeV. This does not occur at 1.35 BeV for the same value of Δ_1^2. Assuming that this effect is not of experimental origin, one possible explanation for this apparent energy

[26] E. Ferrari and F. Selleri, Phys. Rev. Letters **7**, 387 (1961).
[27] In the region where the a and c terms of Eq. (4.1) are negligible.

dependence within the framework of the OPE process is the diffraction-scattering effect of Drell and Hiida.[28] This effect would tend to raise our decay cross section at small angles and large momentum, and would be more pronounced at the higher incident energies (larger average W) where π-p scattering shows a well-developed diffraction peak. Other possibilities include the neglected interference effects of interchanging final state protons, two-pion exchange effects, and final state interactions.

It is difficult to make quantitative statements concerning the higher isobar peaks observed in the experimental data. Their relative insignificance compared to the 3, 3 isobar at small angles is consistent with the OPE theory; this arises from the rapid increase of Δ_1^2 as W increases at a fixed laboratory angle and incident energy. At the large angles this is not longer true, e.g., at 12° and 17° at 2.9 BeV, Δ_1^2 is essentially constant for the first three isobars. It is apparent from the curves of Figs. 6(c), (d), and (e) that the 1.52- and 1.67-BeV isobars are suppressed less than the 3, 3 isobar at the same Δ_1^2, perhaps as much as a factor of 3 less. Stated another way, the cross sections for excitation of the $T=\frac{1}{2}$ isobars do not follow the same function of Δ_1^2 as shown for the 3, 3 isobar in Fig. 12, at least in the region $\Delta_1^2 \sim 20\ \mu^2$ and above.

VI. CONCLUSION

It is concluded that the OPE model, when applied to proton-proton inelastic scattering, gives close agreement with experiment for values of the invariant momentum transfer $\Delta_1^2 \lesssim 6\ \mu^2$ and isobar masses in the neighborhood of 1.23 BeV, the 3, 3 resonance in π-p scattering. However, at larger Δ_1^2 there is a marked deviation from theory. Over the entire range of Δ_1^2 we have been able to fit a smooth "correction factor" $\Gamma^2(\Delta_1^2)$ which is, within the uncertainties of our analysis, independent of incident proton energy. This factor may be related to the "pionic form factor" of the nucleon and "off mass shell" corrections to the π-p scattering amplitudes as proposed by Ferrari and Selleri. From their point of view, the energy independence of this correction factor is considered a requisite to show the dominance, in this reaction, of the single pion exchange process. It is interesting to note that a recent theoretical approach by Frautschi *et al.*[29] based on the concept of Regge poles would predict an energy dependence even for single-pion exchange if the pion is a "composite" particle. In this theory the energy dependence of the cross section coincides with that of the OPE formula only at the one-pion pole, in the physical region the two theories differ. Our data cannot preclude a dependence on energy of less than 20% in the region between 1 and 3 BeV.

The presence in the spectrum of peaks due to excitation of the $T=\frac{1}{2}$ π-p resonances at 600- and 900-MeV laboratory energy has been noted; their general magnitude is consistent with OPE excitation. The dependence of a correction factor on Δ_1^2 is not well determined but it is clearly closer to unity than the correction factor found for the 3, 3 peak. This result is compatible with that of Cocconi *et al.*[30] who find that at incident proton energies between 13 and 26 BeV the 3, 3 peak is absent while the $T=\frac{1}{2}$ peaks persist. This difference in behavior of the $T=\frac{3}{2}$ and $T=\frac{1}{2}$ isobars is suggestive; the one "elementary" particle exchange theory would attribute this to different off-mass-shell corrections or interference contributions from multi-particle exchange; the more recent proposals of "composite" particle exchange would attribute the difference to contributions from different Regge pole trajectories due to the differing isotopic spins of these isobars. The two hypotheses predict different relative behaviors for the isobar cross sections with increasing incident energy; certainly the present data does not allow a choice between these two possibilities; but similar experiments at higher incident energies may provide a feasible test.

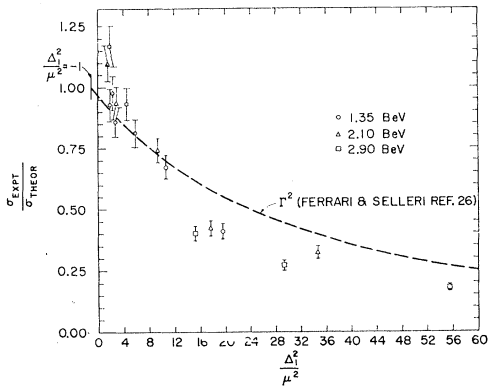

FIG. 12. Ratio of $\sigma_{U,E}$ to the prediction of the OPE model. The dashed curve is the same quantity, as obtained by Ferrari and Selleri (reference 26); see Eq. (5.3) of the text.

ACKNOWLEDGMENTS

We wish to acknowledge the contributions of Professor Sergio deBenedetti and Professor Arthur Roberts who were in the group which initiated these experiments. We wish to thank Dr. Gian Carlo Wick and Professor Robert Serber for assisting us greatly in the interpretation of the one-pion exchange model to our experiments, and, in turn, to thank Dr. R. M. Sternheimer for his interpretations of the isobar model. Finally we wish to express our gratification to the Cosmotron staff for wholehearted cooperation.

One of us (NCH) is grateful to Professor S. deBenedetti for his interest and guidance, and would like to acknowledge helpful discussions with Professor R. Cutkosky.

[28] S. D. Drell and K. Hiida, Phys. Rev. Letters **7**, 199 (1961).
[29] S. C. Frautschi, M. Gell-Mann, and G. Zachariasen, Phys. Rev. **126**, 2204 (1962).
[30] G. Cocconi, A. N. Diddens, E. Lillethun, G. Manning, A. E. Taylor, T. G. Walker, and A. M. Wetherell, Phys. Rev. Letters **7**, 450 (1961).